Neurobiology of Stress 13 (2020) 100253

Contents lists available at ScienceDirect

Neurobiology of Stress

journal homepage: www.elsevier.com/locate/ynstr

Brain-Derived Neurotrophic Factor Val66Met polymorphism interacts with adolescent stress to alter hippocampal interneuron density and dendritic morphology in mice

Rachel Anne Hill [a,b,*], Adrienne Mary Grech [a,b], Michael J. Notaras [b,c], Mauricio Sepulveda [b,d], Maarten van den Buuse [d,e,f]

[a] Department of Psychiatry, School of Clinical Sciences, Monash University, Monash Medical Centre, Clayton, VIC, Australia
[b] The Florey Institute of Neuroscience and Mental Health, University of Melbourne, Parkville, VIC, Australia
[c] Weill Cornell Medical College of Cornell University, Centre for Neurogenetics, Brain & Mind Research Institute, New York City, New York, USA
[d] School of Psychology and Public Health, La Trobe University, Melbourne, VIC, Australia
[e] Department of Pharmacology, University of Melbourne, VIC, Australia
[f] The College of Public Health, Medical and Veterinary Sciences, James Cook University, Townsville, QLD, Australia

ARTICLE INFO

Keywords:
Brain-derived neurotrophic factor
Interneurons
Stress
Hippocampus
Somatostatin

ABSTRACT

Brain-derived neurotrophic factor (BDNF) plays essential roles in GABAergic interneuron development. The common BDNF val66met polymorphism, leads to decreased activity-dependent release of BDNF. The current study used a humanized mouse model of the BDNF val66met polymorphism to determine how reduced activity-dependent release of BDNF, both on its own, and in combination with chronic adolescent stress hormone, impact hippocampal GABAergic interneuron cell density and dendrite morphology.

Male and female Val/Val and Met/Met mice were exposed to corticosterone (CORT) or placebo in their drinking water from weeks 6–8, before brains were perfuse-fixed at 15 weeks. Cell density and dendrite morphology of immunofluorescent labelled inhibitory interneurons; somatostatin, parvalbumin and calretinin in the CA1, and 3 and dentate gyrus (DG) across the dorsal (DHP) and ventral hippocampus (VHP) were assessed by confocal z-stack imaging, and IMARIS dendritic mapping software.

Mice with the Met/Met genotype showed significantly lower somatostatin cell density compared to Val/Val controls in the DHP, and altered somatostatin interneuron dendrite morphology including branch depth, and spine density. Parvalbumin-positive interneurons were unchanged between genotype groups, however BDNF val66met genotype influenced the dendritic volume, branch level and spine density of parvalbumin interneurons differentially across hippocampal subregions. Contrary to this, no such effects were observed for calretinin-positive interneurons. Adolescent exposure to CORT treatment also significantly altered somatostatin and parvalbumin dendrite branch level and the combined effect of Met/Met genotype and CORT treatment significantly reduced somatostatin and parvalbumin dendrite spine density.

In sum, the $BDNF^{Val66Met}$ polymorphism significantly alters somatostatin and parvalbumin-positive interneuron cell development and dendrite morphology. Additionally, we also report a compounding effect of the Met/Met genotype and chronic adolescent CORT treatment on dendrite spine density, indicating that adolescence is a sensitive period of risk for Val66Met polymorphism carriers.

1. Introduction

Brain-Derived Neurotrophic Factor (BDNF) is the most abundant neurotrophic factor expressed in the brain and plays essential roles in neuronal migration, differentiation and survival, as well as activity-dependent synaptic plasticity (von Bohlen Und Halbach and von Bohlen Und Halbach, 2018). BDNF protein can be translated from either short 3′ untranslated region (UTR) transcripts located within the soma or

* Corresponding author. Department of Psychiatry, School of Clinical Sciences at Monash Health, Monash University Level 3, Monash Medical Centre 27Wright St Clayton VIC 3168 Australia, .
E-mail address: Rachel.hill@monash.edu (R.A. Hill).

https://doi.org/10.1016/j.ynstr.2020.100253
Received 27 July 2020; Received in revised form 3 September 2020; Accepted 26 September 2020
Available online 28 September 2020

long 3′ UTR Bdnf transcripts that are targeted to the dendrite, suggesting local actions on the dendrite (An et al., 2008). Indeed, BDNF has important roles in regulating pyramidal cell and interneuron dendritic growth and morphology as well as dendrite spine density both in the cortex and hippocampus (Horch and Katz, 2002; Ji et al., 2005; McAllister et al., 1995; Wirth et al., 2003). However, both enhancing and destabilizing effects of BDNF on dendrite morphology have been shown, and these apparent opposing effects appear to result from different Bdnf splice variants (Maynard et al., 2017).

The common BDNF Val66Met polymorphism is located on the pro-region of BDNF, but has a functional impact on BDNF activity as it disrupts the activity-dependent secretion of BDNF into the synapse by inhibiting sorting of BDNF into secretory granules (Egan et al., 2003) and has been associated with a range of symptom categories and psychiatric illnesses (Chen et al., 2006; Notaras et al., 2015a). In humans, Met/Met carriers show poor episodic memory (Egan et al., 2003), reduced hippocampal volume (Chen et al., 2006) and poorer memory-related hippocampal activity. In Val66Met mice, long-term potentiation and depression were disrupted in the hippocampus of $BDNF^{Met/Met}$ mice compared to $BDNF^{Val/Val}$ control mice (Bath et al., 2012; Ninan et al., 2010). $BDNF^{Met/Met}$ mice furthermore show disruptions in spatial memory (Notaras et al., 2016a), deficits in extinction learning (Dincheva et al., 2012) and a depression-like phenotype (Notaras et al., 2017). $BDNF^{Met/Met}$ mice show epigenetic changes in hippocampal genes involved in dendrite and spine remodelling (*Dvl1, Noc3, Reln*) (Mallei et al., 2018) and reduced dendritic complexity in dentate gyrus neurons (Chen et al., 2006). Furthermore, proteomics analysis shows that the hBDNFVal66Met genotype alters protein levels of many schizophrenia-risk genes (Greening, 2019).

BDNF supports the development and regulates the activity of GABAergic inhibitory interneurons. Signalling via BDNF and its receptor, Tropomyosin-related kinase B (TrkB), directs inhibitory synapse assembly (Chen et al., 2011; Rico et al., 2002), and moderates GABAergic synaptic plasticity (Kohara et al., 2007; Park and Poo, 2013) and neurotransmission (Jovanovic et al., 2004). In mice, BDNF heterozygosity alters inhibitory cell density and protein expression (Du et al., 2018) and disruptions to BDNF-TrkB signalling at inhibitory interneurons can lead to cognitive dysfunction (Grech et al., 2019; Lucas et al., 2014; Xenos et al., 2017). Animal studies have furthermore found that disruptions to inhibitory interneuron development lead to cognitive disruptions in adulthood (Cho et al., 2015) and that silencing of inhibitory interneurons disrupts higher order functioning (Murray et al., 2015). The Val66Met polymorphism in humans is associated with alterations to excitation/inhibition balance (Wiegand et al., 2016) and with hyperexcitability, representing impaired inhibitory regulatory processes (Strube et al., 2015). $BDNF^{Met/Met}$ mice show reduced GABAergic innervation at distal dendrites, but higher at the soma of pyramidal cells in both hippocampal and medial prefrontal cortex regions (Chen et al., 2017).

There are over 20 different subtypes of GABAergic interneurons in the hippocampus, which are classified based on their unique morphology, specific targets (e.g. pyramidal cell or other interneurons), innervation and electrophysiological output, as well as specific molecular markers such as calcium-binding proteins or peptide expression profiles (Kelsom and Lu, 2013). Three main functional classes are identified; perisomatic (interneurons that target the soma of pyramidal cells), dendritic (interneurons that target the dendrite of pyramidal cells) and interneuron-specific (interneurons that target other interneurons) (Booker and Vida, 2018). Human post-mortem studies have found altered expression and cell density of parvalbumin (PV) and somatostatin (SST)-positive GABAergic neurons in prefrontal cortex and hippocampal regions in schizophrenia and bipolar disorder (Fung et al., 2014; Hashimoto et al., 2005; Konradi et al., 2011a). However, the effect of the BDNF Val66Met polymorphism on GABAergic subtype distribution or dendritic morphology within the hippocampus has yet to be comprehensively explored, despite the fact that GABAergic interneurons are critical to the functioning of principle neurons within local hippocampal circuits.

Chronic stress has previously been shown to alter hippocampal GABAergic interneuron cell density in rats (Czeh et al., 2015) and a history of stress hormone exposure modified behavioural outcomes in $hBDNF^{Val66Met}$ mice, including memory function and sensorimotor gating (Notaras et al., 2016a, Notaras, 2016). Furthermore, a recent review showed that the BDNF Val66met polymorphism in humans influences an individual's cortisol responsivity to stress (de Assis and Gasanov, 2019). It is well known that chronic exposure to the major stress hormone, corticosterone (CORT), causes dendritic atrophy in the hippocampus (Woolley et al., 1990) of rodents. However, little is known on whether the interaction of chronic stress and Val66Met genotype on behaviour is associated with changes in interneuron density, and dendritic morphology in the hippocampus.

Given the well-known association between GABAergic dysfunction and cognitive impairment, this study sought to determine whether alterations in hippocampal GABAergic interneuron populations in the BDNFval66met model may provide further understanding of the neurobiological underpinnings that drive our previously identified hippocampal-specific spatial memory deficit found in $hBDNF^{met/met}$ mice.

We therefore assessed hippocampal cell density and dendritic morphology of PV, SST and calretinin (CAL)-positive interneurons in mice with the human $BDNF^{Val66Met}$ polymorphism and chronically treated with CORT during adolescence, to simulate the effects of chronic stress at this critical period of interneuron development (Wu et al., 2014). While a limitation of this study is that mice do not naturally carry this mutation, we have used a humanized mouse model, with both val/val and met/met genotypes aligned with the human BDNF polymorphism, making this model highly translationally relevant. These three subtypes include perisomatic (PV), dendritic (SST) and interneuron-specific (CAL) functional categories, although there is some overlap with PV interneurons being both perisomatic and dendritic.

2. Methods

2.1. Animals

Male and female $hBDNF^{Val66Met}$ mice were generated as previously described (Cao et al., 2007) and offspring used in the current study were obtained from a breeding colony at the Florey Institute, Melbourne, Australia. All mice were on a C57Bl/6 background and $hBDNF^{Val/Met} \times hBDNF^{Val/Met}$ breeding pairs were used to generate Val/Val and Met/-Met littermates. There were 4 groups in this study comprising 2 genotypes ($hBDNF^{Val/Val}$ and $hBDNF^{Met/Met}$), and 2 treatments (water and CORT). Both male and female mice were used. The number of mice per group are shown in Table 1.

Mice were pseudorandomized into the above treatment groups. Males and females were group-housed separately ($n = 2$–6 per box) in individually-ventilated cages (IVC; Tecniplast). The animals had *ad libitum* access to food and water in a temperature-controlled room maintained at approximately 22 °C and on a 12/12-h light/dark cycle. For a period of three weeks starting from 6 weeks of age until 8 weeks of age mice were exposed to 25 mg/L of CORT-hemisuccinate (Q1662-000

Table 1
Mouse grouping and numbers.

Genotype and sex	Adolescent treatment	Number of mice
Val/Val (5 male, 5 female)	water	10
Val/Val (5 male, 5 female)	CORT in drinking water (25 mg/L)	10
Met/Met (4 male, 5 female)	water	9
Met/Met (4 male, 4 female)	CORT in drinking water (25 mg/L)	8

Steraloids Inc, United States) in their drinking water, while control groups received water without CORT. In terms of consumption, in a satellite cohort we found that the average fluid intake over 3 weeks of CORT treatment was 5.6 ml/day/20 g mouse, at a concentration of 25 mg/L. This value was calculated from 6 cages and 16 mice. This method was chosen rather than a stress paradigm for both ethical considerations related to animal stress paradigms and to provide a controlled experiment designed to specifically assess the role of one of the main components of the stress response which is of course multi-factorial. Average body weight of female mice was approximately 21 g while males weighed on average approximately 28 g at 15 weeks of age. Genotype and treatment had no significant effect on body weight. All mice were anaesthetised with a single intraperitoneal injection of 100 µl pentobarbitone diluted 1 in 10 (Virbac, NSW, Australia) at week 15 in the morning (between 9am and 12pm) before transcardial perfusion. All procedures were performed according to guidelines set by the National Health and Medical Research Council of Australia and approved by the Florey Institute for Neuroscience and Mental Health Animal Ethics Committee (16–056) and comply with the ARRIVE guidelines.

2.1.1. Immunhistochemistry

Mice were transcardially perfused with 0.1 M ice-cold phosphate-buffered saline (PBS) (~50 ml) followed by 4% paraformaldehyde in ice-cold 0.1 M PBS (~50 ml). Brains were post-fixed in 4% PFA overnight, transferred to a 15% sucrose solution for 24 h, and then transferred to a 30% sucrose solution for a further 24 h. Brains were snap-frozen and 20 µm coronal sections were cut on a cryostat. Free-floating tissue sections were stored in cryoprotectant (300 ml ethylene glycol, 150 g sucrose, 275 ml dH_2O, 275 ml 0.1 PB pH 7.4) in 24-well cell culture plates. Staining was done in these plates (Costar 3524, Corning Incorporated, Corning, NY, USA) to cause minimal disruption to tissue.

Free-floating tissue sections were sorted to find representative sections of Bregma −1.46, −1.82, −2.18. −2.54, −2.80 and −3.16 mm, to image throughout the dorsal and ventral hippocampus. On Day 1 sections were washed in PB for 10 min on a shaker. PB wash buffer was removed and blocking solution (10% Normal Donkey Serum (NDS) + 1% Triton-X100 in PB) added. Samples were incubated in blocking solution for 1 h at room temperature. Blocking solution was removed and primary antibody solution (primary antibodies + 2% NDS + 0.3% Triton-X100 in PB) added after which the sections were incubated overnight on a rocker at room temperature. On Day 2 samples were washed in PB 3 × 5 min. Samples were then incubated in secondary antibody solution (secondary antibodies + 2% NDS in PB) for 3 h. Following this, samples were washed in PB 3 × 5 min.

Primary antibodies used were: rat anti-SST (1:100, Merck, MAB354), mouse anti-PV (1:1000, Sigma-Aldrich, Sig P30881), rabbit anti-CAL (1:1500, Swant, 7691), and guinea pig anti-NeuN (1:1000, Merck, ABN90). Secondary antibodies used were: donkey anti-rat AlexaFluor 647 (1:200, Jackson Immunoresearch), donkey anti-mouse AlexaFluor 488 (1:400, Jackson Immunoresearch), donkey anti-rabbit AlexaFluor 594 (1:400, Jackson Immunoresearch), and donkey anti-guinea pig Dylight 405 (1:200, Jackson Immunoresearch).

Tissue sections were mounted on glass slides, cover-slipped using Dako Fluorescence Mounting Medium (Dako, North America Inc., CA, USA), and edges sealed with nail polish. Sections were stored at −20 °C. As shown in Figure figs1Supplementary, Fig. 1 and Fig. 2, this method resulted in successful co-labelling of the three interneuron markers; SST (aqua), PV (green), CAL (red), as well as NeuN (blue), with no cross-reactivity or overlap (Fig. 2 and Figs1 Supplementary for zoomed in view). Negative controls included omitting each primary antibody while all secondary antibodies were included.

2.1.2. Stereological cell quantification and image acquisition and analysis

Stacks of images spanning 20 µm in the z-plane were taken in the hippocampal areas to be analysed. DHP samples related to bregma coordinates −1.42, - 1.82 and −2.18 mm, whereas VHP samples related to bregma coordinates −2.54 mm, −280 mm and −3.16 mm. A Nikon C1 confocal microscope with an Andor Zyla 4.2 sCMOS camera was used to capture images at 20x magnification and 3 µm step z-stacks. A maximum projection image was created from each stack using the Nikon C1 confocal software. Expression of markers and area measurements were determined using the FIJI ImageJ 1.52 g software. The experimenter was blinded to mice numbers when counting and determined brain region boundaries based upon NeuN stain. To determine marker expression, a macro was designed for efficient and objective counting. The macro created an individual mask for the 488-PV channel, 647-SST channel and 594-CAL channel. Each of these masks was applied to the 405-NeuN channel to identify co-expression of NeuN with each marker, confirming that the observed immunofluorescence was a neuronal cell. The macro then automatically counted particles between 50 and 300 µm.

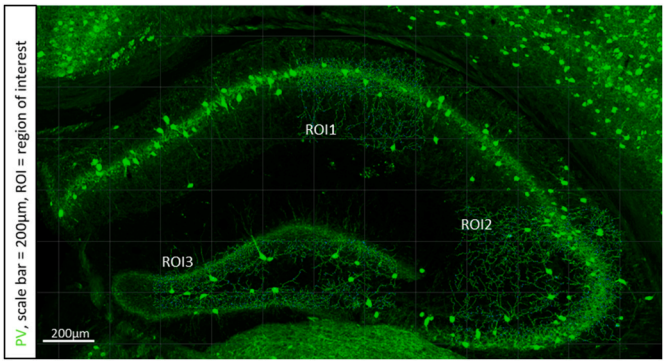

Fig. 1. Representative image of mapped parvalbumin labelled dendrites within designated regions of interest (ROI). ROI-1 corresponds to the CA1 region, ROI-2 the CA3 and ROI-3 the dentate gyrus.

2.1.3. Dendrite morphology and spine density

Dendrite morphology and spine density measures were assessed using IMARIS workstation (x 64, version 9.2.1) with filament tracer and IMARIS XT selection tools. One z-stack image (alternating left and right hemisphere) from the DHP at bregma point 1.82 was assessed per mouse and the assessor was blinded to animal group number. Z-stacks were opened in the Surpass view and the filament tool was selected. Specific regions of interest (ROI) were then defined using the segment region of interest tool. Here ROI-1 corresponded to the CA1 region, with co-ordinates X:747, Y:532. ROI-2 corresponded to the CA3, with co-ordinates X:1000, Y:759 and ROI-3 corresponded to the dentate gyrus (DG), with coordinates X1418, Y388. Z planes were 10 (See Fig. 1 for ROI demarcation in the 488 PV channel). For each fluorescent channel seed points (cell soma) were first detected with parameters set at 20 µm diameter, dendrite diameter set at 2 µm and spine parameters set at 0.8 µm diameter and 3 µm max length. For the 488 channel (PV) dendrite threshold was set at 15.8 and spine threshold at 7.61 for all sections to maintain consistency across animals. For the 647 channel (SST) dendrite threshold was set at 8.37 and spine threshold at 8.3 and for the 594 channel (CAL) dendrite threshold was set at 8.6 and spine threshold at 6.24. The software mapped filaments from each ROI and measured dendrite area (μm^2), length (µm), mean diameter (µm) and volume (μm^3), dendrite branch depth, branch level, and straightness, and dendrite number of spines, and spine density. Dendrite branch depth is the number of branch points or bifurcations in the shortest path from the beginning point to a given point in the dendritic graph. Dendrite branch level is a numerical structure that starts unfolding from the filament beginning toward the terminal points, assigning branching level to dendritic segments at each branching point. Dendritic straightness is the ratio between dendrite length and radial distance between two branch points, with a value of 1 meaning the dendrite is completely straight. All measurements were averaged/ROI/section using R statistical program. For PV labelled dendrites the number of mapped dendrites ranged from

1200 to 3400 within the CA1 region, from 2100 to 6000 in the CA3 and from 2900 to 6500 in the DG. For SST the number of mapped dendrites were much lower with 50–200 in CA1, 400–3000 in CA3 and 150–2400 in DG. For CAL the number of mapped dendrites ranged from 30 to 1000 in CA1, 120–4500 in CA3 and 1000–4500 in DG. There were no group differences in the number of mapped dendrites.

2.2. Statistical analysis

All data are presented as mean ± the standard error of the mean (SEM). Outliers were identified using the ROUT test with Q = 1% (Graphpad PRISM software). D'Agostino-Pearson tests were performed to confirm data are normally distributed. Cell density and outputs of dendrite morphology were first assessed using a repeated-measures ANOVA with region as the within-subject variable and genotype, treatment and sex as the between-subject factors. For all cell density measurements there were no interactions with sex, so data for the sexes were collapsed. For all dendrite morphology measures except spine density and number of spines there was no effect of sex, and no interaction of sex with genotype or CORT treatment. However, for spine density measurements significant interactions between sex and treatment or genotype were found for PV and calretinin, therefore sexes were analysed separately here.

Three-way repeated measures ANOVA or mixed-effects model with hippocampal subregions (CA1, CA3, DG), as the matching factor and genotype and treatment as the independent variables was then applied to either collapsed sex data sets or separated male and female data sets for spine density. If region interacted with genotype, or treatment, data were split accordingly and analysed by two-way ANOVAs using Graphpad PRISM software with Sidak's multiple comparison where justified. Group differences were considered significant when $p < 0.05$.

3. Results

3.1. Cell density dorsal hippocampus

Analysis of SST cell density in the DHP showed a significant main effect of genotype F (1, 33) = 7.662, P = 0.0092) with $hBDNF^{Met/Met}$ mice showing reduced cell density compared to $hBDNF^{Val/Val}$ (Fig. 2A and D). No significant effect of CORT treatment (F (1, 33) = 0.1239, P = 0.72) on SST cell density was found and there was no significant CORT × genotype interaction (F (1, 33) = 0.009, p = 0.92). There was a main effect of region (F (1.712, 56.50) = 197.8, P < 0.0001) with significantly lower SST density in the DG compared to the CA1 (p < 0.0001) and CA3 (P < 0.0001) regions (Fig. 2A and D). No significant effects of genotype (F (1, 34) = 1.302, P = 0.26) or CORT treatment (F (1, 34) = 3.509, P = 0.06) or genotype × CORT interactions (F (1, 34) = 0.1276, P = 0.72) were found for PV (Fig. 2B). No significant effect of genotype (F (1, 33) = 0.9429, p = 0.33), CORT treatment (F (1, 33) = 1.368, P = 0.25) or genotype × CORT interactions (F (1, 33) = 1.824, P = 0.18) were found for CAL (Fig. 2C) cell density in the DHP. A main effect of region was found for PV (F (2, 67) = 268.0, P < 0.0001) with significantly lower cell density in the DG compared to CA1 (P < 0.0001) and CA3 (P < 0.0001) (Fig. 2B and E), while for CAL interneurons the highest density was found in the DG (main effect of region F (1.928, 63.63) = 178.7, P < 0.0001) with levels significantly higher than CA1 (P < 0.0001) and CA3 (P < 0.0001) (Fig. 2C and E).

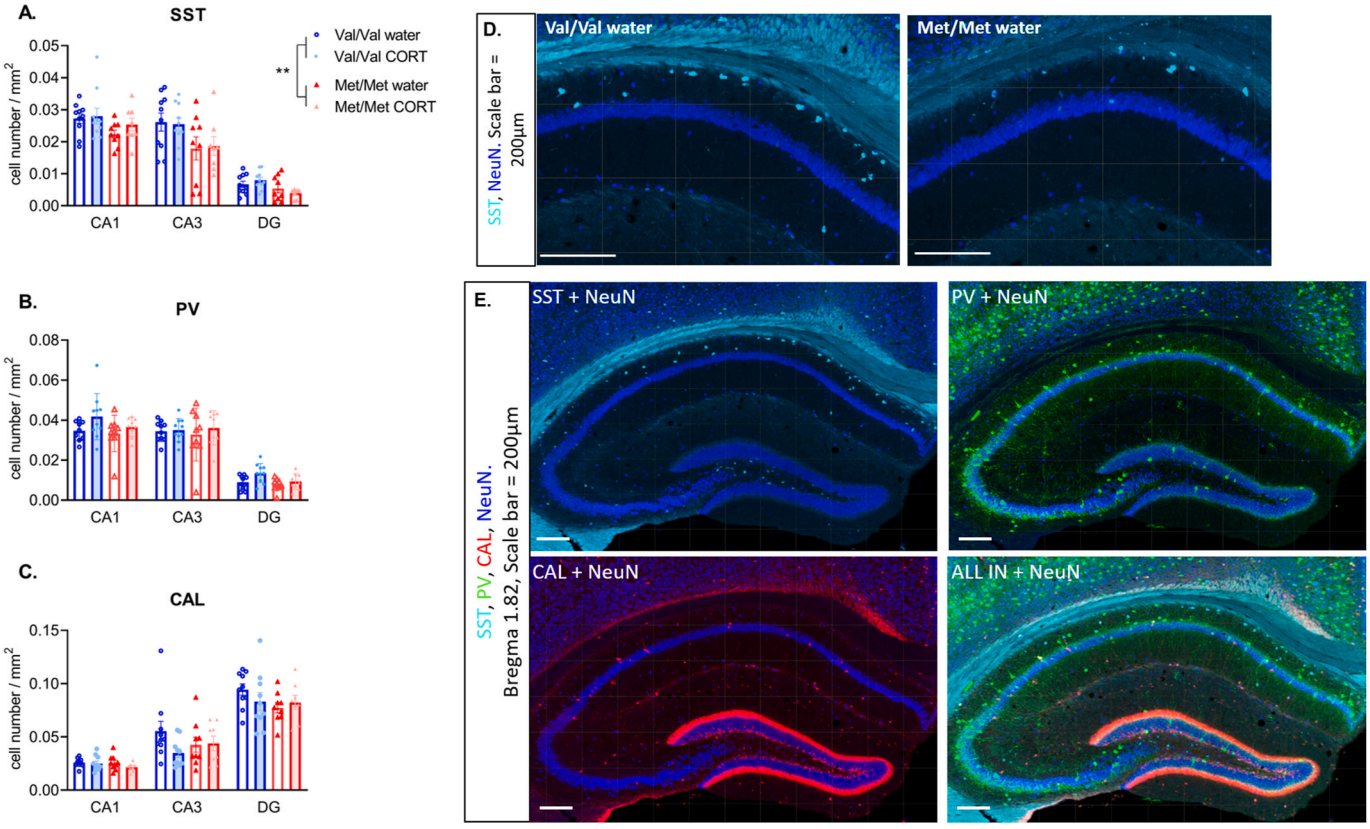

Fig. 2. Average interneuron cell density across the DHP in $hBDNF^{Val/Val}$ and $hBDNF^{Met/Met}$ mice that were either control (water) or CORT-treated. **A)** SST cell density is significantly reduced in $hBDNF^{Met/Met}$ compared to $hBDNF^{Val/Val}$ mice. **B)** PV cell density is unchanged by genotype, or CORT treatment, **C)** CAL cell density is unchanged by genotype, or CORT treatment. ** next to met/met legend indicates significant main effect of genotype ($p < 0.01$). N = 9–10/group. Panel **D)** show representative images of somatostatin in the CA1 of Val/Val water and Met/Met water treated mice, scale bar = 100 µm. Panel **E)** Shows all 3 interneurons + NeuN labelling in a Val/Val water treated (control) mouse, scale bar = 200 µm.

3.1.1. Cell density ventral hippocampus

No significant effects of genotype ($F(1, 32) = 0.6382$, $P = 0.43$), CORT treatment ($F(1,32) = 1.44$, $p = 0.23$) or genotype × CORT interaction ($F(1,32) = 1.78$, $P = 0.19$) were found for SST cell density in the VHP (Fig. 3A). No significant effect of genotype ($F(1,32) = 0.63$, $P = 0.43$), CORT treatment ($F(1, 32) = 1.443$, $P = 0.23$) or genotype × CORT interaction ($F(1, 32) = 1.782$, $P = 0.19$) was found for PV cell density in the VHP (Fig. 3B).

However, there was a main effect of region ($F(1.988, 61.62) = 24.44$, $p < 0.0001$), with significantly higher SST cell density levels in the CA1 compared to the CA3 ($p < 0.0001$) and DG ($p < 0.0001$) (Fig. 3A and E). For PV there was a main effect of region ($F(1.580, 50.57) = 81.72$, $p < 0.0001$), with significantly higher levels of PV cell density in the CA3 compared to CA1 ($P = 0.0049$) and DG ($P < 0.0001$) and significantly higher PV cell density in CA1 compared to DG ($P < 0.0001$) (Fig. 3B and E).

For CAL cell density in the VHP there was no main effect of genotype ($F(1, 32) = 3.689$, $P = 0.06$) or treatment ($F(1,32) = 0.94$, $P = 0.33$) but a significant region × treatment interaction was found ($F(2, 64) = 6.313$, $P = 0.0031$), with CORT significantly reducing CAL cell density within the CA3 region (main effect of CORT treatment in CA3 $F(1, 32) = 5.451$, $P = 0.026$) (Fig. 3C and D). In addition there was a main effect of region ($F(1.478, 47.28) = 69.19$, $P < 0.0001$) with CAL cell density significantly higher in the DG compared to CA1 ($P < 0.0001$) and CA3 ($P < 0.0001$).

3.1.2. SST interneuron dendrite morphology

Dendrite volume, area and length: Dendrite volume, branch level and spine density are shown graphically in Fig. 4. For dendrite volume no main effect of genotype ($F(1,26) = 0.07$, $P = 0.78$) or treatment ($F(1,26) = 0.28$, $P = 0.69$) was found and no significant interactions ($F(1,26) = 0.33$, $P = 0.56$). There was however, a main effect of region, with the DG showing lower dendrite volume compared to CA1 ($P = 0.025$) and CA3 ($P = 0.023$) (Fig. 4A). Dendrite area and length were also unchanged by genotype, treatment or sex (Table 2).

Dendrite branch level, depth and straightness: For dendrite branch level there was a significant effect of genotype ($F(1, 28) = 8.147$, $P = 0.008$) and treatment ($F(1, 28) = 6.046$, $P = 0.02$) but no genotype × treatment interaction ($F(1,28) = 0.27$, $P = 0.6$). Here the $hBDNF^{Met/Met}$ genotype reduced but CORT treatment increased SST dendrite branch level (Fig. 4B and D). There was also a main effect of genotype for dendrite branch depth ($F(1, 25) = 4.330$, $P = 0.04$), again with $hBDNF^{Met/Met}$ mice showing reduced branch depth (Table 2). Dendrite straightness was unchanged by genotype or treatment.

Dendrite spine density and number of spines: For dendrite spine density there was a main effect of genotype ($F(1, 29) = 6.966$, $P = 0.01$), but no effect of treatment ($F(1,29) = 0.32$, $P = 0.57$). However, there was a region x genotype × treatment interaction ($F(2, 58) = 3.234$, $P = 0.04$). Here, the $hBDNF^{Met/Met}$ genotype showed reduced dendrite spine density, specifically within the CA3 ($F(1, 14) = 10.45$, $P = 0.006$) and DG ($F(1, 29) = 7.298$, $P = 0.01$) but not the CA1 (Fig. 4C and D). Furthermore, within the CA3 there was a treatment × genotype interaction ($F(1, 14) = 6.530$, $P = 0.022$) with the $hBDNF^{Met/Met}$ CORT group showing significantly reduced spine density compared to the $hBDNF^{Met/Met}$ water treated group ($P = 0.002$) (Fig. 4C and D). There was a main effect of genotype for dendrite number of spines ($F(1, 28) = 4.266$, $P = 0.04$) (Table 2), again with the $hBDNF^{Met/Met}$ genotype showing reduced dendrite number of spines compared to $hBDNF^{Val/Val}$. However, there was no effect of treatment and no treatment × genotype interaction for number of spines.

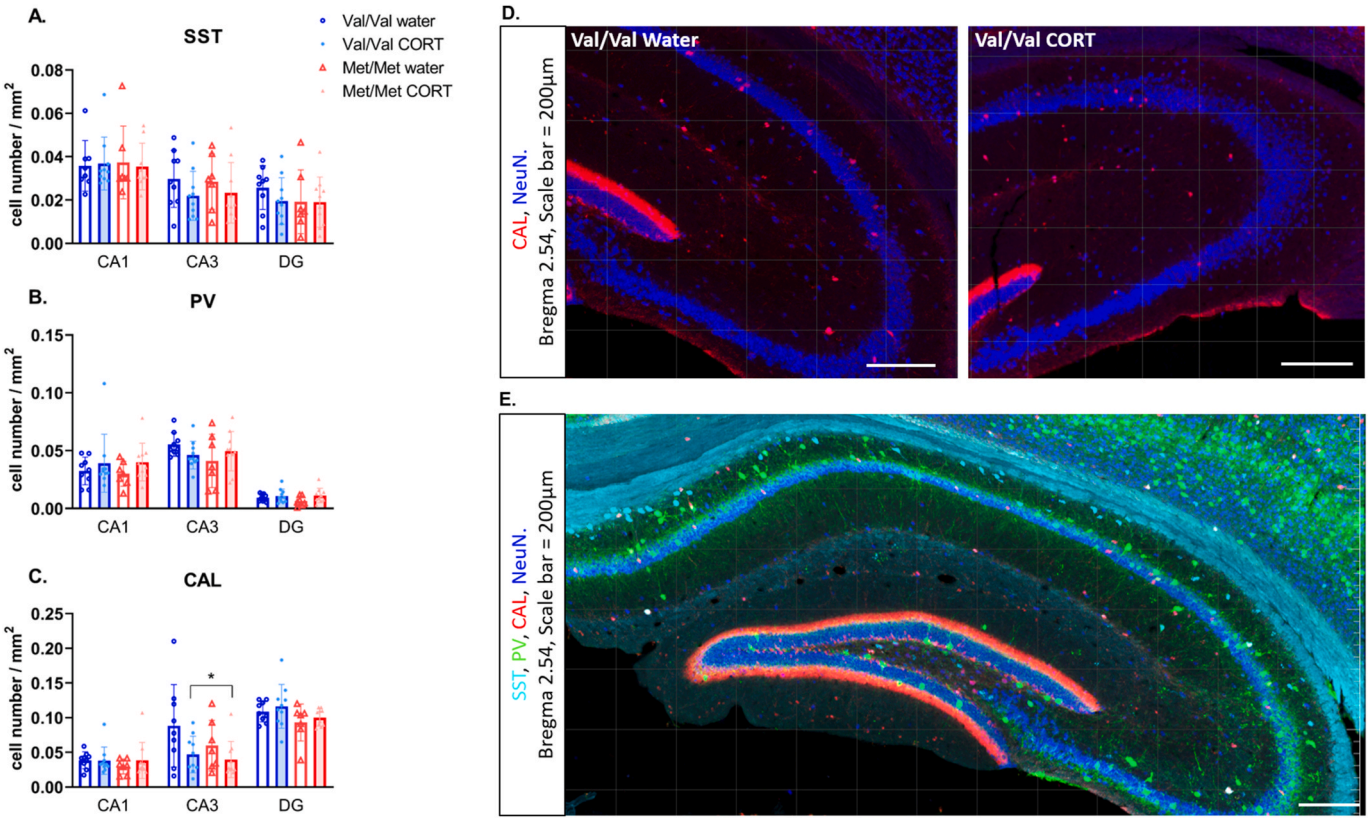

Fig. 3. Average interneuron cell density across the VHP in $hBDNF^{Val/Val}$ and $hBDNF^{Met/Met}$ mice that were control (water) or CORT-treated. **A)** SST cell density is unchanged by genotype or CORT treatment, **B)** PV cell density is unchanged by genotype or CORT treatment, **C)** CAL cell density is unchanged by genotype, but CORT treatment reduced cell density in the CA3. * over lines indicates significant effect of CORT treatment. N = 9–10/group. **D)** Representative image of calretinin staining in the CA3 of water and CORT treated Val/Val mice. Panel **E)** Shows all 3 interneurons + NeuN labelling. Scale bar = 200 µm.

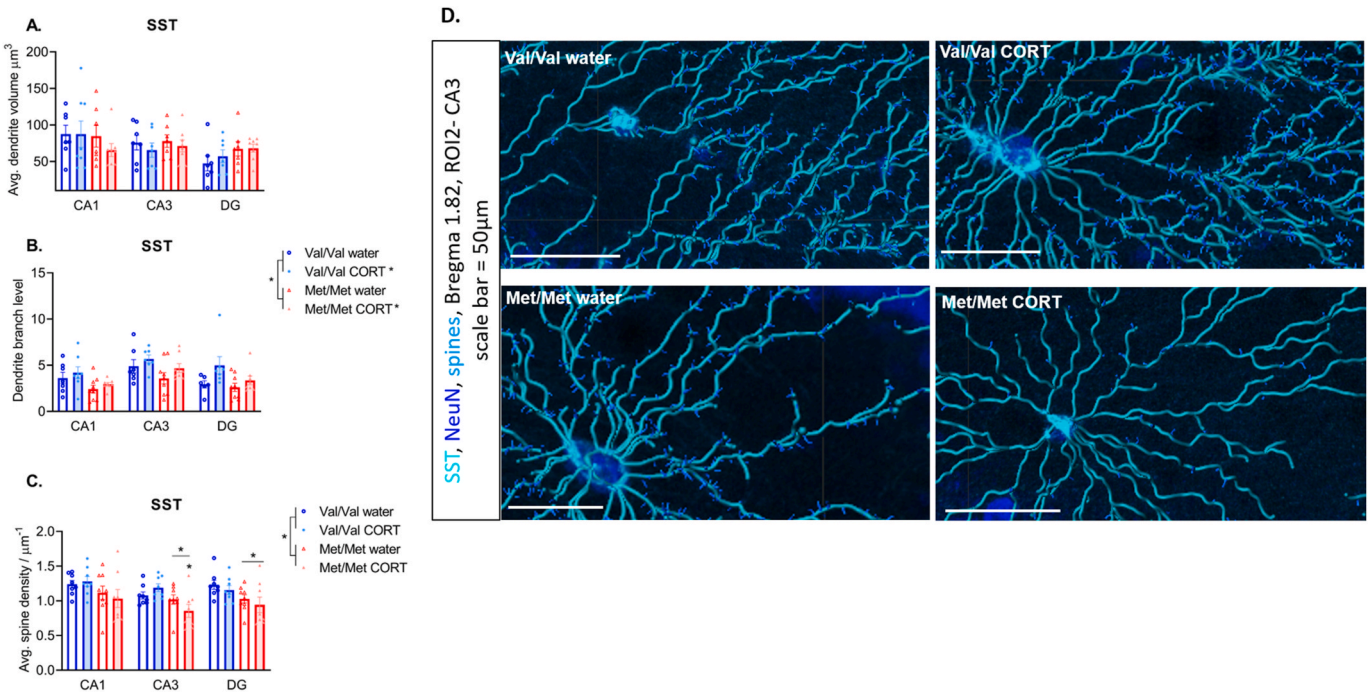

Fig. 4. Somatostatin interneuron dendrite morphology. **A**) Dendrite volume is unchanged by genotype or CORT treatment, **B**) Significant effects of genotype and CORT were found for dendrite branch level, and **C**) Significant genotype x treatment x region effects were found for dendrite spine density with the Met/Met mice exposed to CORT showing the lowest dendrite spine density. * next to lines linking genotypes in legend indicate main effect of genotype, * next to CORT groups in legend indicate main effect of CORT, * above lines in graph indicate main effects of genotype within subregions, * above Met/Met + CORT group indicate interaction of treatment x genotype within the CA3 subregion. N = 7–9/group. Panel **D**) shows representative images of mapped dendrites and dendritic spines within the CA3 region, scale bar = 50 µm.

Table 2
Dendrite morphology somatostatin interneurons. Data are mean ± SEM. * = P < 0.05.

Group	Val/Val control	Val/Val CORT	Met/Met control	Met/Met CORT
Dendrite length µm				
CA1	24.88 ± 3.09	24.41 ± 5.37	24.14 ± 4.42	18.67 ± 2.38
CA3	21.46 ± 2.83	18.38 ± 2.50	23.04 ± 2.49	20.82 ± 2.42
DG	22.03 ± 4.38	21.47 ± 3.88	29.03 ± 5.25	27.49 ± 2.51
Dendrite Area µm^2				
CA1	160.66 ± 20.4	160.09 ± 34	156.22 ± 28.7	120.26 ± 15.5
CA3	136.5 ± 18.2	116.9 ± 16.1	146.8 ± 16.0	132.8 ± 15.5
DG	142.8 ± 29.3	137.0 ± 24.8	188.7 ± 35.6	178.4 ± 17.0
Dendrite diameter µm				
CA1	2.1 ± 0.03	2.07 ± 0.04	2.09 ± 0.03	2.07 ± 0.02
CA3	2.04 ± 0.01	2.04 ± 0.01	2.04 ± 0.01	2.05 ± 0.007
DG	2.07 ± 0.02	2.06 ± 0.01	2.08 ± 0.02	2.11 ± 0.02
Dendrite branch depth * **main effect of genotype**				
CA1	6.50 ± 1.89	7.07 ± 1.71	4.69 ± 1.22 *	4.42 ± 0.50*
CA3	8.44 ± 1.36	11.25 ± 1.37	7.19 ± 4.13 *	8.8 ± 1.66 *
DG	4.44 ± 1.01	8.95 ± 1.68	4.27 ± 0.98 *	5.28 ± 1.25 *
Dendrite straightness – 1 = straight				
CA1	0.89 ± 0.003	0.89 ± 0.009	0.89 ± 0.008	0.90 ± 0.004
CA3	0.90 ± 0.004	0.90 ± 0.002	0.90 ± 0.002	0.90 ± 0.003
DG	0.89 ± 0.002	0.90 ± 0.002	0.88 ± 0.007	0.89 ± 0.003
Dendrite No. of Spines * **main effect of genotype**				
CA1	1.92 ± 0.76	3.2 ± 1.93	0.57 ± 0.29 *	0.99 ± 0.27 *
CA3	1.2 ± 0.34	1.02 ± 0.34	0.48 ± 0.16 *	0.95 ± 0.16 *
DG	2.5 ± 1.05	2.33 ± 1.05	1.65 ± 1.28 *	1.17 ± 0.24 *

3.1.3. PV interneuron dendrite morphology

Dendrite volume, area and length: For PV interneuron dendrite volume there was no main effect of genotype (F (1,29) = 2.1, P = 0.15) or treatment F (1,29) = 1.5, P = 0.22) and no genotype × treatment interaction (F (1,29) = 0.12, P = 0.73). However, there was a region × genotype interaction (F (2, 58) = 0.6887, P = 0.01), with the main effect of genotype specifically found in CA1 (F (1, 29) = 4.880, P = 0.03) with hBDNF$^{Met/Met}$ mice showing reduced volume compared to hBDNF$^{Val/Val}$ (Fig. 5A). A significant region × genotype interaction was also found for dendrite area (F (2, 58) = 4.536, P = 0.01), again with the main effect of genotype specifically found in CA1 (F (1, 29) = 5.388, P = 0.02) (Table 3). Dendrite length was unchanged by genotype or treatment (Table 3).

Dendrite branch level, depth and straightness: For dendrite branch level, however, there was no effect of genotype (F (1,29) = 0.01, P = 0.9), but a significant effect of treatment (F (1, 29) = 4.402, P = 0.04) and a significant region × treatment interaction (F (2, 58) = 3.703, p = 0.03). Here, CORT treatment reduced parvalbumin dendrite branch level specifically within the DG (F (1, 29) = 4.749, P = 0.03) (Fig. 5B). Dendrite branch depth and straightness were unchanged by genotype or treatment (Table 3).

Dendrite spine density and number of spines: For dendrite spine density, 4-way ANOVA showed a significant treatment × sex interaction (F (1,29) = 0.83, P = 0.007). Therefore, we split the sexes for this analysis. In male mice, no significant effect of genotype (F (1,11) = 0.84, P = 0.37), treatment (F (1,11) = 1.7, P = 0.21) or genotype × treatment interaction was found (F (1,11) = 0.02, P = 0.87) (Fig. 5C). However, in female mice there was a significant main effect of genotype (F (1,14) = 23.7, P = 0.0002), a significant main effect of treatment (F (1,14) = 12.11, P = 0.0037) and a significant genotype × treatment interaction (F (1,14) = 4.69, P = 0.048) (Fig. 5D). Here both hBDNF$^{met/met}$ genotype and CORT treatment reduce spine density in female mice with the two-hit effect causing the lowest spine density across all subregions of the hippocampus.

Similarly, for number of dendrite spines, there was a trend for a treatment × sex interaction (F (1,29) = 0.2, P = 0.053), therefore the sexes were split for this analysis. Once again, in male mice, there was no effect of genotype (F (1,11) = 0.78, P = 0.39), treatment (F (1,11) =

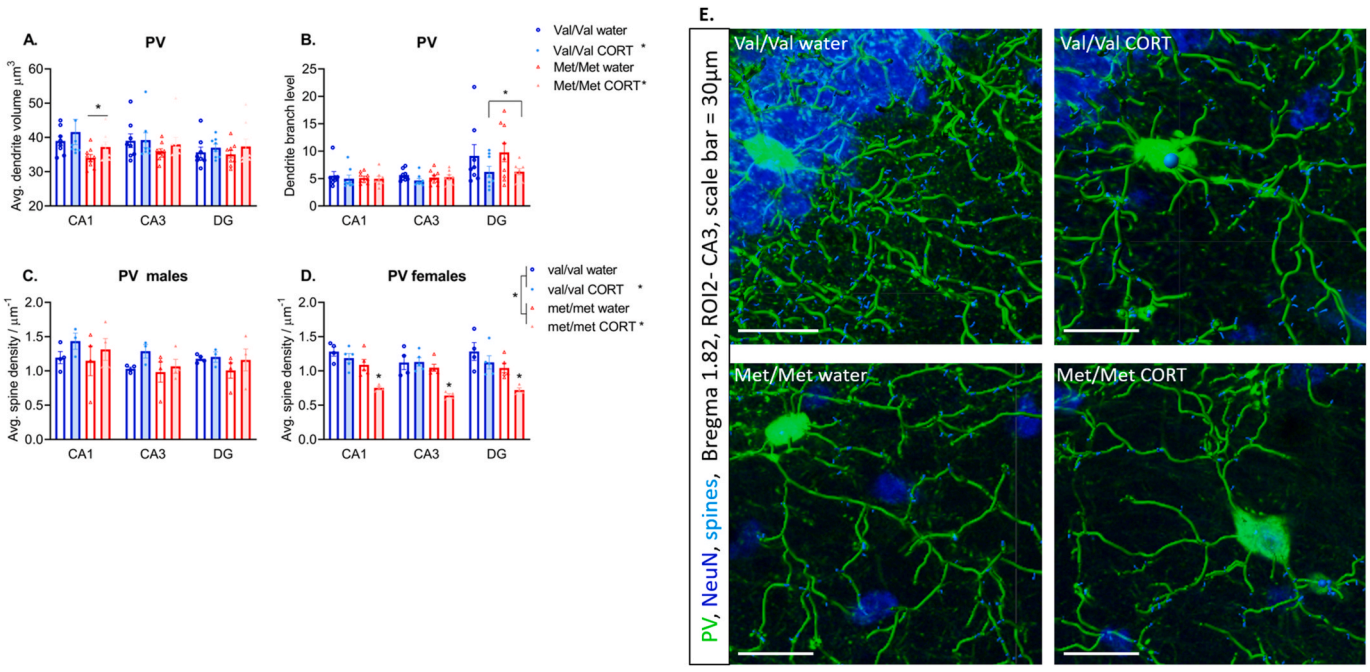

Fig. 5. Parvalbumin interneuron dendrite morphology. **A**) Dendrite volume is reduced in Met/Met mice in the CA1, and **B**) CORT treatment reduced dendrite branch level in DG. Significant sex x treatment effects were found for parvalbumin spine density therefore sexes were split. Male mice show no significant effect of genotype, treatment or interaction for spine density **C**), however, females two-hit mice show reduced spine density **D**). N = 7–9/group. Panel **E**) shows mapped parvalbumin dendrites and dendritic spines in the CA3 region of female mice, scale bar = 30 µm.

Table 3
Dendrite morphology parvalbumin interneurons.

Group	Val/Val control	Val/Val CORT	Met/Met control	Met/Met CORT
Dendrite length µm				
CA1	12.14 ± 0.39	12.82 ± 0.93	10.67 ± 0.31	11.61 ± 0.41
CA3	12.16 ± 0.61	12.15 ± 0.57	11.28 ± 0.25	11.81 ± 0.56
DG	11.06 ± 0.39	11.49 ± 0.32	11.12 ± 0.35	11.66 ± 0.64
Dendrite Area µm^2 * **region x genotype**				
CA1 *	76.96 ± 2.58	81.59 ± 6.35	67.36 ± 2.05 *	73.59 ± 2.72 *
CA3	77.15 ± 3.92	77.23 ± 3.85	71.38 ± 1.68	74.94 ± 3.78
DG	70.24 ± 2.70	72.97 ± 2.00	70.22 ± 2.30	73.90 ± 4.19
Dendrite diameter µm				
CA1	2.03 ± 0.008	2.04 ± 0.022	2.01 ± 0.004	2.02 ± 0.009
CA3	2.03 ± 0.006	2.03 ± 0.008	2.01 ± 0.007	2.03 ± 0.009
DG	2.03 ± 0.01	2.03 ± 0.009	2.011 ± 0.004	2.02 ± 0.006
Dendrite branch depth				
CA1	11.33 ± 2.28	10.59 ± 1.63	11.02 ± 0.48	9.78 ± 0.79
CA3	10.34 ± 0.87	9.30 ± 0.45	10.64 ± 1.00	10.36 ± 0.98
DG	21.68 ± 7.11	13.69 ± 2.62	24.5 ± 5.81	13.61 ± 2.03
Dendrite straightness - 1 = straight				
CA1	0.899 ± 0.002	0.905 ± 0.001	0.907 ± 0.0007	0.901 ± 0.002
CA3	0.899 ± 0.003	0.903 ± 0.001	0.903 ± 0.001	0.901 ± 0.002
DG	0.900 ± 0.002	0.903 ± 0.003	0.901 ± 0.001	0.900 ± 0.003
Dendrite No. of Spines **Males**				
CA1	1.69 ± 0.2	2.03 ± 0.2	1.44 ± 0.3	1.88 ± 0.3
CA3	1.4 ± 0.9	1.8 ± 0.25	1.2 ± 0.19	1.51 ± 0.34
DG	1.41 ± 0.17	1.53 ± 0.12	1.21 ± 0.16	1.63 ± 0.4
Dendrite No. of Spines **Females** *main effect of genotype				
CA1	1.87 ± 0.23	1.90 ± 0.2	1.32 ± 0.11 *	0.87 ± 0.02 *
CA3	1.54 ± 0.2	1.57 ± 0.23	1.25 ± 0.07 *	0.75 ± 0.02 *
DG	1.53 ± 0.2	1.4 ± 0.13	1.21 ± 0.07 *	0.8 ± 0.03 *

Data are mean ± SEM. * = P < 0.05.

2.68, P = 0.12) or genotype × treatment interaction (F (1,11) = 0.036, P = 0.86). However, females showed a significant effect of genotype with hBDNF$^{Met/Met}$ mice showing reduced number of dendritic spines (F (1,14) = 17.23, P = 0.001) compared to hBDNF$^{Val/Val}$. No effect of treatment (F (1,14) = 2.7, P = 0.11) and no genotype × treatment interaction (F (1,14) = 2.22, P = 0.15) was found for number of dendritic spines in female mice. (Table 3).

3.1.4. CAL interneuron dendrite morphology

Dendrite volume, area and length: No significant effects of genotype (F (1,29) = 3.2, P = 0.9) or CORT treatment (F (1,29) = 0.004, P = 0.94) and no genotype × CORT interaction (F (1,29) = 0.69, P = 0.4) was found for CAL interneuron dendrite volume (Fig. 6A). Area and length were also unchanged by genotype or treatment (Table 4). There was a main effect of region for dendrite volume (F (1.494, 43.33) = 42.18, P < 0.0001), with the DG showing lower dendrite volume compared to CA1 (P < 0.0001) and CA3 (P < 0.0001) (Fig. 6A). Similarly, a main effect of region was found for dendrite area (F (1.492, 43.28) = 42.23, P < 0.0001), again with the DG showing lower dendrite area compared to CA1 (P < 0.0001) and CA3 (P < 0.0001) (Table 4).

Dendrite branch level, depth and straightness: No effect of genotype (F (1,29) = 4.1, P = 0.06), treatment (F (1,29) = 1.8, P = 0.99), region or genotype × treatment interactions (F (1,29) = 0.87, P = 0.35) were found for calretinin dendrite branch level (Fig. 6B). Branch depth and straightness were also unchanged by genotype or treatment (Table 4).

Dendrite spine density and number of spines: For dendrite spine density there was no effect of genotype (F (1,29) = 4.23, P = 0.05) or treatment (F (1,29) = 0.008, P = 0.93) and no genotype × treatment interaction (F (1,29) = 3.1, P = 0.09). However, we did find a significant genotype x sex (F (1,29) = 5.5, P = 0.026) and treatment x sex (F (1,29) = 8.1, P = 0.008) interaction. Therefore, males and females were split and analysed separately.

For male mice there was no significant effect of genotype (F (1,11) = 0.05, P = 0.8), but CORT treatment significantly increased dendrite spine density (F (1,11) = 5.4, P = 0.04), while there was no genotype × treatment interaction (F (1,11) = 0.16, P = 0.7) (Fig. 6C). In addition, there was a significant region × treatment interaction (F (2,22) = 4.1, P = 0.03), and so the regions were split and two-way ANOVA was performed for male mice at each region with genotype and treatment as fixed effects. Here, the main effect of CORT treatment increasing spine

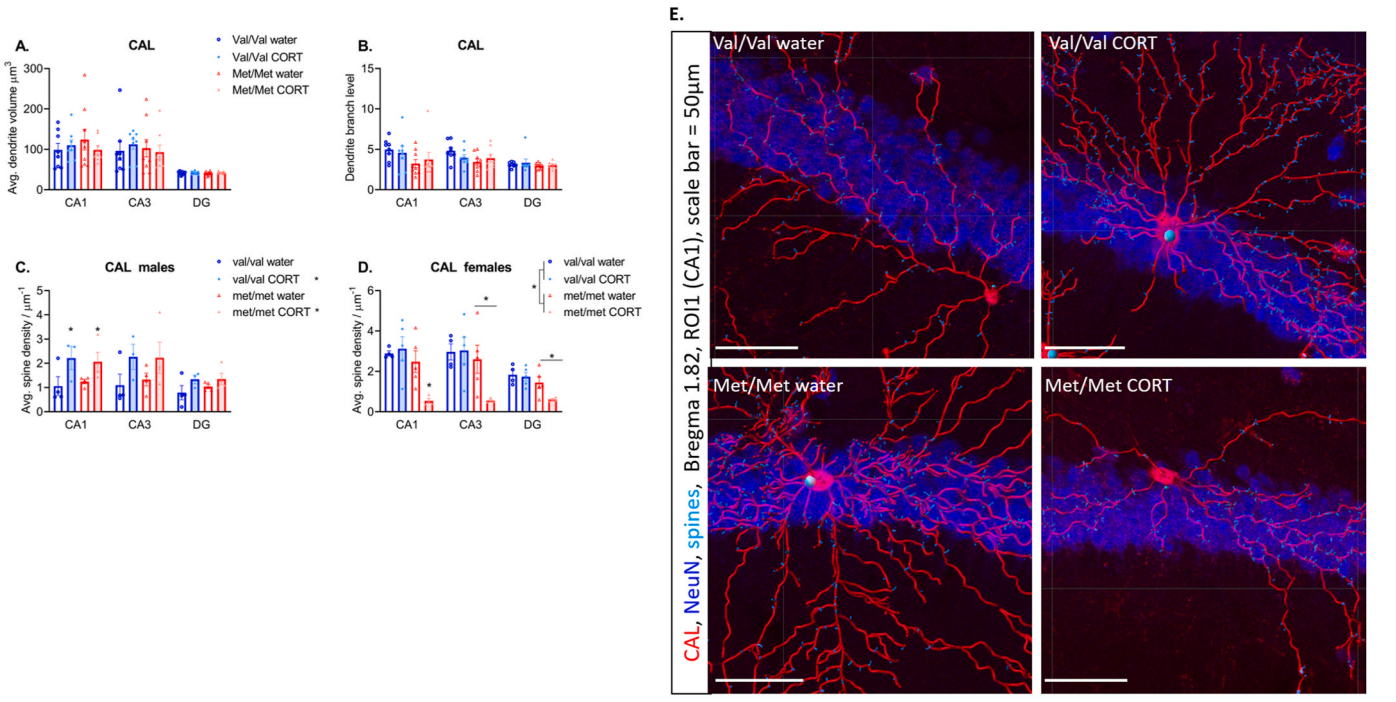

Fig. 6. Calretinin interneuron dendrite morphology. **A**) Dendrite volume, and **B**) Dendrite branch level are unchanged. Significant sex x treatment effects were found for CAL spine density therefore sexes were split. Males show no differences in spine density **C**) however, females two-hit mice show reduced spine density, particularly within the CA1. N = 7–9/group. Panel **E**) shows mapped calretinin dendrites and dendritic spines in the CA1 region of female mice, scale bar = 50 µm.

Table 4
Dendrite morphology calretinin interneurons.

Group	Val/Val control	Val/Val CORT	Met/Met control	Met/Met CORT
Dendrite length µm				
CA1	28.96 ± 3.95	29.1 ± 3.75	33.56 ± 6.01	27 .08 ± 2.8
CA3	28.83 ± 6.3	31.62 ± 4.06	30.16 ± 5.64	25.99 ± 4.43
DG	12.25 ± 0.36	12.16 ± 0.38	11.92 ± 0.22	12.36 ± 0.22
Dendrite Area µm^2				
CA1	188.33 ± 26.05	189.87 ± 26.05	221.64 ± 40.96	177.32 ± 18.41
CA3	185.92 ± 40.88	204.89 ± 26.46	195.75 ± 37.38	168.79 ± 29.32
DG	79.99 ± 2.49	79.45 ± 2.68	77.83 ± 1.77	81.09 ± 1.50
Dendrite diameter µm				
CA1	2.13 ± 0.039	2.12 ± 0.029	2.19 ± 0.047	2.18 ± 0.028
CA3	2.02 ± 0.007	2.11 ± 0.023	2.11 ± 0.0305	2.13 ± 0.038
DG	2.09 ± 0.009	2.09 ± 0.012	2.08 ± 0.011	2.10 ± 0.0017
Dendrite branch depth				
CA1	8.12 ± 1.10	6.45 ± 1.27	4.67 ± 1.21	5.88 ± 2.07
CA3	7.38 ± 0.84	6.09 ± 0.94	5.45 ± 1.12	5.71 ± 0.87
DG	4.61 ± 0.32	5.93 ± 1.58	4.72 ± 0.26	4.50 ± 0.10
Dendrite straightness – 1 = straight				
CA1	0.89 ± 0.003	0.89 ± 0.003	0.88 ± 0.004	0.89 ± 0.005
CA3	0.89 ± 0.003	0.88 ± 0.003	0.88 ± 0.005	0.89 ± 0.004
DG	0.91 ± 0.002	0.92 ± 0.003	0.91 ± 0.003	0.91 ± 0.002
Dendrite No. of Spines **Males** * **Main effect of treatment**				
CA1	2.43 ± 1.1	6.28 ± 1.5 *	3.44 ± 0.96	6.95 ± 2.51 *
CA3	2.8 ± 1.5	8.7 ± 3.2 *	3.68 ± 1.47	9.0 ± 5.46 *
DG	1.2 ± 0.55	2.3 ± 0.46 *	1.59 ± 0.17	2.4 ± 0.56 *
Dendrite No. of Spines **Females**				
CA1	12 ± 2.4	12.46 ± 3.7	12.6 ± 4.0	1.42 ± 0.21
CA3	14.3 ± 5.0	11.9 ± 2.9	12.5 ± 4.6	1.65 ± 0.14
DG	3.25 ± 0.41	2.86 ± 0.47	2.38 ± 0.52	0.86 ± 0.05

Data are mean ± SEM. * = P < 0.05.

density was significant in the CA1 (F (1,6) = 7.6, P = 0.03), but not in the CA3 (F (1,6) = 4.3, P = 0.08), or DG (F (1,6) = 3.7, P = 0.1) suggesting the effect of CORT treatment in the males appears to be most pronounced in the CA1 region (Fig. 6C). No significant effect of genotype (F (1,5) = 0.002, P = 0.96) and no genotype × treatment interaction (F (1,6) = 0.2, P = 0.65) was found in the CA1, CA3, genotype (F (1,5) = 0.04, P = 0.85) and genotype × treatment interaction (F (1,5) = 0.07, P = 0.8) or DG, genotype (F (1,6) = 3.6, P = 0.5), and genotype × treatment interaction (F (1,5) = 0.3, P = 0.6).

In female mice, the met/met genotype once again caused a significant reduction in dendrite spine density (F (1,14) = 8.9, P = 0.009), while there was no effect of treatment (F (1,14) = 3.5, P = 0.08) and no treatment × genotype interaction (F (1,14) = 4.1, P = 0.07) (Fig. 6D). In addition, we found a significant region x genotype × treatment interaction for female mice (F (2,28) = 3.9, P = 0.03). Therefore, we further separated the females by region and performed a two-way ANOVA for each region, with genotype and treatment as the fixed effects. Here, there was a significant effect of genotype (F (1,14) = 10.4, P = 0.006) and a significant treatment x genotype effect (F (1,14) = 5.5, P = 0.03) in the CA1. Post-hoc comparisons showed that the significant effect of CORT was only present in hBDNF$^{met/met}$ mice with this two-hit group showing the lowest spine density (Fig. 6D and E). In the CA3 region there was a significant main effect of genotype (F (1,6) = 6.6, P = 0.04), but no effect of treatment (F (1,6) = 2.9, P = 0.1) and no treatment × genotype interaction (F (1,8) = 2.9, P = 0.12). Again, with hBDNF$^{met/met}$ mice show reduced spine density. Similarly, in the CA3, there was a main effect of genotype (F (1,6) = 26, P = 0.002) with hBDNF$^{met/met}$ showing reduced spine density, but no effect of treatment (F (1,6) = 3.4, P = 0.1) and no treatment × genotype interaction (F (1,6) = 3.5, P = 0.1).

For number of spines there was no main effect of genotype (F (1,29) = 1.4, P = 0.25), treatment (F (1,29) = 0.8, P = 0.77) or genotype × treatment interaction (F (1,29) = 1.45, P = 0.24). However, there was a significant sex × treatment interaction (F (1,29) = 6.1, P = 0.02). Therefore, the sexes were analysed separately. Here male mice showed a significant effect of treatment (F (1,12) = 5.3, P = 0.04), whereby CORT treatment increased number of dendritic spines. However, there was no effect of genotype (F (1,12) = 0.0007, P = 0.93) and no genotype × treatment interaction (F (1,12) = 0.13, P = 0.72) (Table 4). In female mice there was no significant effect of genotype (F (1,14) = 3.1, P =

0.09), treatment (F (1,14) = 0.32, P = 0.09) and no genotype × treatment interaction (F (1,14) = 2.2), P = 0.15) (Table 4).

4. Discussion

This study investigated the effects of Val66Met genotype and a history of adolescent stress hormone exposure on inhibitory interneuron density and dendrite morphology in the dorsal and ventral hippocampus. Our main findings were that in the DHP, but not the VHP, $hBDNF^{Met/Met}$ mice exhibited a robust reduction in SST cell density, irrespective of prior CORT treatment. BDNF Val66Met genotype also had profound effects on SST and PV-positive interneuron dendrite morphology, including branch depth, volume and spine density, with no such effects found for CAL-positive interneurons. Adolescent CORT treatment also significantly altered SST and PV dendrite branch level and the combined effect of Met/Met genotype and CORT treatment significantly reduced SST and PV dendrite spine density.

BDNF has previously been shown to be important in regulating SST gene expression in the prefrontal cortex (Glorioso et al., 2006) and BDNF treatment in striatal (Mizuno et al., 1994) and hippocampal cultures (Marty and Onteniente, 1999) increases SST levels and the number of SST-immunoreactive neurons, respectively. Recently we reported that both male and female BDNF heterozygous mice show decreased mPFC SST density at 12 weeks compared to 4 weeks, indicating developmental interactions with BDNF genotype in the PFC (Du et al., 2018). These findings support the notion that BDNF is important for the development of normal SST cell density across forebrain regions. Disruptions to somatostatin-positive interneurons have been reported in both schizophrenia and bipolar disorder, in both cortical and hippocampal regions (Fung et al., 2014; Konradi et al., 2011a, 2011b; Morris et al., 2008). Disruptions to hippocampal GABAergic interneurons are thought to underlie some of the cognitive impairments found clinically in schizophrenia (Heckers and Konradi, 2015).

We have previously shown deficits in spatial memory (Y-maze) as well as contextual and cued fear memory in $hBDNF^{Met/Met}$ compared to $hBDNF^{Val/Val}$ mice, which are behaviours strongly reliant upon intact dorsal hippocampus functioning (Notaras et al., 2016a). SST interneurons have been shown to be an important part of CA1 inhibitory circuits that govern contextual fear conditioning (Lovett-Barron et al., 2014). Optogenetic inhibition of SST disrupted spatial encoding and reduced hippocampal-prefrontal synchrony (Abbas et al., 2018). SST interneurons in the DG have also been reported to play an essential role in the formation of granule cell assemblies during memory acquisition, particularly in the context of spatial information (Yuan et al., 2017). Our study suggests that spatial and context-dependent memory deficits in $hBDNF^{Met/Met}$ mice may be related to a reduction in SST cell density in the CA1, CA3 and DG of the DHP.

We also found significant effects of genotype on SST and PV dendrite branch level and spine density, with $hBDNF^{Met/Met}$ mice showing reduced dendrite branching and spine density. Our labelling shows that the majority of SST-positive cells reside in the Stratum Oriens layer with horizontal spiny dendrites as previously reported (Booker and Vida, 2018). These cells mainly target principal cell dendritic shafts, provide prototypical feedback inhibition on pyramidal cells (Maccaferri, 2005) and regulate theta frequency local field potential oscillations (Cammalleri et al., 2019; Goldin et al., 2007).

PV-positive interneurons can be perisomatic basket cells, axo-axonic cells or bistratified with somata residing in the stratum pyramidale or proximal stratum oriens and radiatum (Booker and Vida, 2018), and dendrites reported to extend vertically in all layers of the CA1. Our images (Figs. 1 and 2E) show extensive parvalbumin positive cell labelling within the pyramidal layer with fewer cells in the stratum oriens and radiatum. Mapped dendrites within the CA1 pyramidal layer show vertical extensions into the radiatum layer as previously reported (Booker and Vida, 2018). Horizontal bistratified cells tend to express both SST and PV with small secondary dendrites. A limitation of our study is that we did not differentiate between perisomatic basket cells, axo-axonic cells or bistratified cells thus our data represent the average of all PV-labelled dendrites. PV-positive interneurons provide rapid feedback inhibition to pyramidal cells, and regulate high-frequency gamma oscillations (Colgin et al., 2009; Sohal et al., 2009) and knockdown of the BDNF receptor, TrkB, on parvalbumin interneurons disrupts oscillatory activity (Xenos et al., 2017). In addition, BDNF heterozygous mice show impaired gamma oscillations (Jones, 2017). The functional consequences of reduced SST and PV dendrite spine density and branching found here are likely to influence feedback inhibition of pyramidal cells and theta and gamma oscillations should be further explored in this model in future studies. Our data provide further evidence that the Val66Met genotype disrupts the excitatory:inhibitory balance, as previously reported in human studies (Wiegand et al., 2016), and further add to this literature by showing that a major contributor to this disruption is a reduction in inhibitory interneuron SST cell density and SST and PV dendrite morphology. Previous reports by Ninan et al. show disrupted NMDA receptor neurotransmission within the CA1 pyramidal neurons of BDNF met/met mice (Ninan et al., 2010). Given that SST and PV interneurons synapse onto pyramidal neurons in the CA1 and regulate their firing via feedback inhibition, our data support this previous finding and provide further evidence that both excitatory and inhibitory neurons are altered by this genotype.

While previous studies have reported that chronic stress alters hippocampal interneuron density (Czeh et al., 2015) in rodents, our model of chronic CORT treatment during adolescence showed no effects on PV, SST or CAL cell density in the DHP, but a selective reduction in CAL interneurons in the CA3 region of the VHP. While CORT treatment had a negative impact on dendrite spine density both for SST and PV-positive interneurons, it increased dendrite branching of SST-positive interneurons. Given the prominent role that SST interneurons play in spatial and context-dependent memories, this positive effect of CORT on dendrite branch level, may provide some clues as to why treatment of $hBDNF^{Met/Met}$ mice with corticosterone improved spatial memory deficits (Notaras et al., 2016a), albeit this two-hit group showed significantly reduced dendrite spine density.

A limitation of this study is that we did not stain for glutamate decarboxylase (GAD), the enzyme that synthesizes GABA (Pinal and Tobin, 1998) and is generally used as a marker for inhibitory interneurons (Engel et al., 2001). We were limited by how many channels could be imaged by the confocal equipment, and chose to instead use NeuN as a cell-body marker. This allowed for the broader hippocampal structures to be imaged and the relative fields of integrated interneurons. The literature indicates that the majority of hippocampal interneurons expressing our primary markers (SST, PV, and Cal) are indeed inhibitory (DeFelipe et al., 2013; Freund and Buzsáki, 1996; Gonchar and Burkhalter, 1997). In addition, the segmentation tool for dendritic mapping did not easily allow for layer-specific mapping of dendrites of the hippocampus. We were thus unable to further define layer-specific alterations. Furthermore, spine density subtypes (stubby, mushroom and filopodium) were unable to be identified. However, our results indicate that our data still exhibit cell-type specificity, as the dendritic morphology of CAL-positive interneurons were spared when compared to SST and PV-positive interneurons. Another limitation of this study is that this polymorphism is naturally occurring in humans but not mice, thus the regulatory processes that lead to GABAergic dysfunction may differ across species. These needs to be considered when interpreting this animal model data.

In conclusion, our results show that $hBDNF^{Val/Met}$ genotype is a critical modifier of SST cell density, as well as SST and PV interneuron dendrite morphology. While the Met/Met genotype and a history of adolescent CORT exposure produced a compounding effect upon dendrite spine density, we also found that CORT treatment selectively increased dendrite branching of SST interneurons. The $hBDNF^{Val66Met}$ genotype and chronic adolescent stress have been implicated in a broad range of psychiatric disorders particularly in regards to cognitive deficits

(Chao et al., 2008). Our data therefore shed new light on the functional relevance of this common polymorphism and vulnerability to stress, which may interact to alter behaviours related to psychiatric disorders. Indeed, the compounding effects of being met/met and exposed to CORT on dendrite spine density may, in part, explain the observations in humans of differential response to a history of stress or excess cortisol on a number of functional and behavioural measures (de Assis and Gasanov, 2019; Notaras et al., 2015b).

Author contributions and acknowledgments

RAH performed all dendrite mapping and data analysis and wrote the manuscript. AMG performed the immunohistochemistry and confocal microscopy studies and initial data analysis and drafted the manuscript. MJN performed all *in vivo* experiments, including mouse CORT treatments, and perfuse-fixations and edited the manuscript. MS sectioned and pretreated the brains. MvdB and RH funded and co-designed the project and edited the manuscript.

The authors wish to acknowledge the help of Dr. Shane Cheung, and Dr Giulia Ballerin, Monash Micro Imaging – MHTP, The Hudson Institute of Medical Research, for development of the macro used for immunohistochemistry analysis and for assistance with the IMARIS software. The authors would like to acknowledge One in Five philanthropic organization for their support. RAH was supported by a NHMRC Career Development Fellowship. MJN was supported by a NHMRC CJ Martin Fellowship. MvdB was supported by a NHMRC Senior Research Fellowship and Research Focus Area grant funding from La Trobe University.

Conflicts of interest

The authors have no competing interests.

CRediT authorship contribution statement

Rachel Anne Hill: Conceptualization, Methodology, Software, Formal analysis, Data curation, Writing - original draft, Writing - review & editing, Supervision, Funding acquisition. **Adrienne Mary Grech:** Methodology, Formal analysis, Data curation, Writing - original draft. **Michael J. Notaras:** Methodology, Writing - review & editing. **Mauricio Sepulveda:** Methodology. **Maarten van den Buuse:** Conceptualization, Writing - review & editing, Supervision, Funding acquisition.

Appendix A. Supplementary data

Supplementary data to this article can be found online at https://doi.org/10.1016/j.ynstr.2020.100253.

References

Abbas, A.I., et al., 2018. Somatostatin interneurons facilitate hippocampal-prefrontal synchrony and prefrontal spatial encoding. Neuron 100, 926–939 e3.
An, J.J., et al., 2008. Distinct role of long 3' UTR BDNF mRNA in spine morphology and synaptic plasticity in hippocampal neurons. Cell 134, 175–187.
Bath, K.G., et al., 2012. BDNF Val66Met impairs fluoxetine-induced enhancement of adult hippocampus plasticity. Neuropsychopharmacology 37, 1297–1304.
Booker, S.A., Vida, I., 2018. Morphological diversity and connectivity of hippocampal interneurons. Cell Tissue Res. 373, 619–641.
Cammalleri, M., et al., 2019. Molecular and cellular mechanisms underlying somatostatin-based signaling in two model neural networks, the retina and the Hippocampus. Int. J. Mol. Sci. 20.
Cao, L., et al., 2007. Genetic modulation of BDNF signaling affects the outcome of axonal competition in vivo. Curr. Biol. 17, 911–921.
Chao, H.M., et al., 2008. BDNF Val66Met variant and age of onset in schizophrenia. Am. J. Med. Genet. Part B: Neuropsychiatric Genetics 147B, 505–506.
Chen, A.I., et al., 2011. TrkB (tropomyosin-related kinase B) controls the assembly and maintenance of GABAergic synapses in the cerebellar cortex. J. Neurosci. 31, 2769–2780.
Chen, Y.W., et al., 2017. Variant BDNF-Val66Met polymorphism is associated with layer-specific alterations in GABAergic innervation of pyramidal neurons, elevated anxiety and reduced vulnerability of adolescent male mice to activity-based anorexia. Cerebr. Cortex 27, 3980–3993.
Chen, Z.Y., et al., 2006. Genetic variant BDNF (Val66Met) polymorphism alters anxiety-related behavior. Science 314, 140–143.
Cho, K.K., et al., 2015. Gamma rhythms link prefrontal interneuron dysfunction with cognitive inflexibility in Dlx5/6(+/-) mice. Neuron 85, 1332–1343.
Colgin, L.L., et al., 2009. Frequency of gamma oscillations routes flow of information in the hippocampus. Nature 462, 353–357.
Czeh, B., et al., 2015. Chronic stress reduces the number of GABAergic interneurons in the adult rat hippocampus, dorsal-ventral and region-specific differences. Hippocampus 25, 393–405.
de Assis, G.G., Gasanov, E.V., 2019. BDNF and Cortisol integrative system - plasticity vs. degeneration: Implications of the Val66Met polymorphism. Front. Neuroendocrinol. 55, 100784.
DeFelipe, J., et al., 2013. New insights into the classification and nomenclature of cortical GABAergic interneurons. Nat. Rev. Neurosci. 14, 202–216.
Dincheva, I., et al., 2012. Impact of the BDNF Val66Met polymorphism on cognition: Implications for behavioral genetics. Neuroscientist 18, 439–451.
Du, X., et al., 2018. Prefrontal cortical parvalbumin and somatostatin expression and cell density increase during adolescence and are modified by BDNF and sex. Mol. Cell. Neurosci. 88, 177–188.
Egan, M.F., et al., 2003. The BDNF val66met polymorphism affects activity-dependent secretion of BDNF and human memory and hippocampal function. Cell 112, 257–269.
Engel, D., et al., 2001. Plasticity of rat central inhibitory synapses through GABA metabolism. J. Physiol. 535, 473–482.
Freund, T.F., Buzsáki, G., 1996. Interneurons of the hippocampus. Hippocampus 6, 347–470.
Fung, S.J., et al., 2014. Schizophrenia and bipolar disorder show both common and distinct changes in cortical interneuron markers. Schizophr. Res. 155, 26–30.
Glorioso, C., et al., 2006. Specificity and timing of neocortical transcriptome changes in response to BDNF gene ablation during embryogenesis or adulthood. Mol. Psychiatr. 11, 633.
Goldin, M., et al., 2007. Synaptic kainate receptors tune oriens-lacunosum moleculare interneurons to operate at theta frequency. J. Neurosci. 27, 9560–9572.
Gonchar, Y., Burkhalter, A., 1997. Three distinct families of GABAergic neurons in rat visual cortex. Cerebr. Cortex 7, 347–358.
Grech, A.M., et al., 2019. Sex-specific spatial memory deficits in mice with a conditional TrkB deletion on parvalbumin interneurons. Behav. Brain Res. 372, 111984.
Greening, D.W., et al., 2019. Chronic methamphetamine interacts with BDNF Val66Met to remodel psychosis pathways in the mesocorticolimbic proteome. Mol. Psychiatr. https://doi.org/10.1038/s41380-019-0617-8.
Hashimoto, T., et al., 2005. Relationship of brain-derived neurotrophic factor and its receptor TrkB to altered inhibitory prefrontal circuitry in schizophrenia. J. Neurosci. 25, 372–383.
Heckers, S., Konradi, C., 2015. GABAergic mechanisms of hippocampal hyperactivity in schizophrenia. Schizophr. Res. 167, 4–11.
Horch, H.W., Katz, L.C., 2002. BDNF release from single cells elicits local dendritic growth in nearby neurons. Nat. Neurosci. 5, 1177–1184.
Ji, Y., et al., 2005. Cyclic AMP controls BDNF-induced TrkB phosphorylation and dendritic spine formation in mature hippocampal neurons. Nat. Neurosci. 8, 164–172.
Jones, N.C., et al., 2017. Brain-derived neurotrophic factor haploinsufficiency impairs high-frequency cortical oscillations in mice. Eur. J. Neurosci. 48 (8), 2816–2825.
Jovanovic, J.N., et al., 2004. Brain-derived neurotrophic factor modulates fast synaptic inhibition by regulating GABA(A) receptor phosphorylation, activity, and cell-surface stability. J. Neurosci. 24, 522–530.
Kelsom, C., Lu, W., 2013. Development and specification of GABAergic cortical interneurons. Cell Biosci. 3, 19.
Kohara, K., et al., 2007. A local reduction in cortical GABAergic synapses after a loss of endogenous brain-derived neurotrophic factor, as revealed by single-cell gene knock-out method. J. Neurosci. 27, 7234–7244.
Konradi, C., et al., 2011a. Hippocampal interneurons are abnormal in schizophrenia. Schizophr. Res. 131, 165–173.
Konradi, C., et al., 2011b. Hippocampal interneurons in bipolar disorder. Arch. Gen. Psychiatr. 68, 340–350.
Lovett-Barron, M., et al., 2014. Dendritic inhibition in the hippocampus supports fear learning. Science 343, 857–863.
Lucas, E.K., et al., 2014. Mice lacking TrkB in parvalbumin-positive cells exhibit sexually dimorphic behavioral phenotypes. Behav. Brain Res. 274, 219–225.
Maccaferri, G., 2005. Stratum oriens horizontal interneurone diversity and hippocampal network dynamics. J. Physiol. 562, 73–80.
Mallei, A., et al., 2018. Global epigenetic analysis of BDNF Val66Met mice hippocampus reveals changes in dendrite and spine remodeling genes. Hippocampus 28, 783–795.
Marty, S., Onteniente, B., 1999. BDNF and NT-4 differentiate two pathways in the modulation of neuropeptide protein levels in postnatal hippocampal interneurons. Eur. J. Neurosci. 11, 1647–1656.
Maynard, K.R., et al., 2017. Bdnf mRNA splice variants differentially impact CA1 and CA3 dendrite complexity and spine morphology in the hippocampus. Brain Struct. Funct. 222, 3295–3307.
McAllister, A.K., et al., 1995. Neurotrophins regulate dendritic growth in developing visual cortex. Neuron 15, 791–803.
Mizuno, K., et al., 1994. Brain-derived neurotrophic factor promotes differentiation of striatal GABAergic neurons. Dev. Biol. 165, 243–256.

Morris, H.M., et al., 2008. Alterations in somatostatin mRNA expression in the dorsolateral prefrontal cortex of subjects with schizophrenia or schizoaffective disorder. Cerebr. Cortex 18, 1575–1587.
Murray, A.J., et al., 2015. Parvalbumin-positive interneurons of the prefrontal cortex support working memory and cognitive flexibility. Sci. Rep. 5, 16778.
Ninan, I., et al., 2010. The BDNF Val66Met polymorphism impairs NMDA receptor-dependent synaptic plasticity in the hippocampus. J. Neurosci. 30, 8866–8870.
Notaras, M.J., et al., 2016. BDNF Val66Met genotype interacts with a history of simulated stress exposure to regulate sensorimotor gating and startle reactivity. Schizophr. Bull. 43 (3), 665–672.
Notaras, M., et al., 2017. The BDNF Val66Met polymorphism regulates glucocorticoid-induced corticohippocampal remodeling and behavioral despair. Transl. Psychiatry 7, e1233.
Notaras, M., et al., 2016a. BDNF Val66Met genotype determines hippocampus-dependent behavior via sensitivity to glucocorticoid signaling. Mol. Psychiatr. 21, 730–732.
Notaras, M., et al., 2015a. The BDNF gene Val66Met polymorphism as a modifier of psychiatric disorder susceptibility: progress and controversy. Mol. Psychiatr. 20, 916–930.
Notaras, M., et al., 2015b. A role for the BDNF gene Val66Met polymorphism in schizophrenia? A comprehensive review. Neurosci Biobehav Rev.
Park, H., Poo, M.-M., 2013. Neurotrophin regulation of neural circuit development and function. Nat. Rev. Neurosci. 14, 7–23.
Pinal, C.S., Tobin, A.J., 1998. Uniqueness and redundancy in GABA production. Perspect. Dev. Neurobiol. 5, 109–118.
Rico, B., et al., 2002. TrkB receptor signaling is required for establishment of GABAergic synapses in the cerebellum. Nat. Neurosci. 5, 225–233.
Sohal, V.S., et al., 2009. Parvalbumin neurons and gamma rhythms enhance cortical circuit performance. Nature 459, 698–702.
Strube, W., et al., 2015. BDNF-Val66Met-polymorphism impact on cortical plasticity in schizophrenia patients: A proof-of-concept study. Int. J. Neuropsychopharmacol. 18, pyu040.
von Bohlen Und Halbach, O., von Bohlen Und Halbach, V., 2018. BDNF effects on dendritic spine morphology and hippocampal function. Cell Tissue Res. 373, 729–741.
Wiegand, A., et al., 2016. Genetic modulation of transcranial direct current stimulation effects on cognition. Front. Hum. Neurosci. 10, 651.
Wirth, M.J., et al., 2003. Accelerated dendritic development of rat cortical pyramidal cells and interneurons after biolistic transfection with BDNF and NT4/5. Development 130, 5827–5838.
Woolley, C.S., et al., 1990. Exposure to excess glucocorticoids alters dendritic morphology of adult hippocampal pyramidal neurons. Brain Res. 531, 225–231.
Wu, Y.C., et al., 2014. Sex differences in the adolescent developmental trajectory of parvalbumin interneurons in the hippocampus: a role for estradiol. Psychoneuroendocrinology 45, 167–178.
Xenos, D., et al., 2017. Loss of TrkB signaling in parvalbumin-expressing basket cells results in network activity disruption and abnormal behavior. Cerebr. Cortex 1–15.
Yuan, M., et al., 2017. Somatostatin-positive interneurons in the dentate gyrus of mice provide local- and long-range septal synaptic inhibition. Elife 6, e21105.